Iranian Journal of Astronomy and Astrophysics
Vol. 12, No. 4, Autumn 2025, 323–334
©Available online at http://ijaa.du.ac.ir
DOI: 10.22128/ijaa.2026.3282.1245
Online ISSN: 2383–403X

Iranian Journal of Astronomy and Astrophysics

Research Paper

Time-Series Forecasting of Geomagnetic Activity: A Data-Driven Approach for K_{p} Index Prediction

Sevim Ranjbar[1] · Somayeh Taran*[2]

[1] Faculty of Physics, University of Tabriz, PO Box 51666-16471, Tabriz, Iran;
E-mail: sevimranjbar1403@ms.tabrizu.ac.ir

[2] Faculty of Physics, University of Tabriz, PO Box 51666-16471, Tabriz, Iran;
*E-mail: taran@tabrizu.ac.ir

Received: 25 February 2026; **Accepted:** 26 May 2026; **Published:** 30 May 2026

Abstract. The geomagnetic index K_{p} is a fundamental metric for quantifying geomagnetic activity and understanding solar-terrestrial physics. Accurately modeling and predicting its nonlinear fluctuations remains a significant challenge in the study of space climate. In this research, we propose a robust statistical approach using a Long Short Term Memory (LSTM) neural network for the time series forecasting of the K_{p} index. Our models are trained and evaluated on a comprehensive dataset spanning a 25 year period from 1999 to 2024, utilizing high resolution solar wind data sourced from the NASA OMNIWeb database. We incorporate eight critical physical parameters as input features, including three dimensional magnetic field components and plasma properties. A critical aspect of sequential modeling is determining the optimal historical context. Therefore, we systematically evaluate the impact of various input time windows (6, 12, 24, 48, 72, and 120 hours) on the predictive performance of the network. Our empirical analysis reveals that the 6 hour input window yields the highest precision, achieving an R^2 score of 0.7233 and minimizing the root mean square error (RMSE). These results indicate that short term solar memory contains the most relevant dynamical features for forecasting geomagnetic variations. This study highlights the effectiveness of LSTM architectures in capturing the short term dynamical evolution of the Earth's magnetic environment, offering valuable insights for future data driven research in space physics.

Keywords: Geomagnetic K_{p} Index, Time Series Forecasting, Long Short Term Memory (LSTM), Solar-Terrestrial Physics, Statistical Modeling.

1 Introduction

The K_{p} index is one of the most widely used global indicators of geomagnetic activity driven by solar–terrestrial interactions that provides a standardized three hourly logarithmic measure of disturbances in the horizontal component of the Earth's magnetic field derived from a network of mid latitude geomagnetic observatories [1,2]. The K_{p} index reflects the integrated response of the magnetosphere to solar wind forcing and serves as a fundamental proxy for space weather conditions that is extensively employed in studies of magnetospheric dynamics, space climate variability, and operational forecasting systems [3–5].

* *Corresponding author*

Variations in geomagnetic activity are primarily controlled by solar wind plasma properties and interplanetary magnetic field (IMF) conditions measured upstream of Earth's magnetosphere [6–8]. Numerous observational and modeling studies demonstrate strong statistical coupling between geomagnetic disturbances and key solar wind parameters such as solar wind velocity, IMF magnitude, and the southward IMF component [9–11]. Time shifted solar wind datasets enable consistent analysis of solar wind–magnetosphere coupling by propagating upstream measurements to the Earth's bow shock nose [12,13]. These datasets form the basis of many modern space weather prediction frameworks and provide long term, homogeneous records suitable for data driven modeling approaches [14,15].

Forecasting geomagnetic activity remains a challenging problem due to the nonlinear, multiscale dynamics of the coupled solar wind–magnetosphere system [16]. Early prediction efforts relied primarily on empirical relationships and linear statistical techniques that attempted to map solar wind inputs to geomagnetic responses [17–20]. While such approaches provide valuable physical insights, they are limited in their ability to represent the nonlinear feedback processes, time dependencies, and regime transitions inherent in magnetospheric dynamics [19].

Researchers have increasingly adopted machine learning methods as statistical tools for geomagnetic prediction to overcome these limitations. Previous studies demonstrate that Artificial Neural Networks (ANNs) improve performance over classical statistical models by capturing nonlinear relationships between solar wind drivers and geomagnetic indices [21,22]. Furthermore, recent computational advances enable scientists to apply deep learning architectures specifically designed for sequential and time dependent data analysis. Time series forecasting algorithms, particularly LSTM model, show strong predictive capability for geomagnetic indices by preserving temporal dependencies and learning complex dynamical patterns directly from observational data [23,24].

Despite the demonstrated effectiveness of LSTM based forecasting frameworks, an important modeling factor that remains insufficiently explored is the selection of the historical input window length [25,26]. The window size determines the extent of past solar wind information incorporated into the prediction process and directly influences both the physical interpretability and statistical performance of the model. An insufficient window may omit relevant magnetospheric memory effects, whereas an excessively long window may introduce noise and degrade predictive skill due to nonstationary solar wind conditions [27–30]. Determining an optimal temporal context for geomagnetic forecasting therefore, represents a critical step toward improving model robustness and advancing data driven space weather prediction methodologies. Furthermore, recent studies on the complexity of time series have demonstrated that geomagnetic indices, including K_p, exhibit significant long term correlated memory and self affinity, necessitating advanced nonlinear modeling approaches [31].

In this paper, we systematically investigate the impact of various temporal window lengths on the accuracy of K_p index forecasting using an LSTM architecture. We evaluate time windows ranging for $w = 6, 12, 24, 48, 72$,and 120 to identify the optimal historical context required for precise predictions. The remainder of this paper is structured as follows: Section 2 details the dataset. Section 3 describes the Sliding Time Window Construction, LSTM neural network Architecture, Network Architecture and Training Configuration, and Evaluation Metrics (e.g., RMSE, MAE, and R^2). Sections 4 and 5 illustrate the results and conclusion, respectively.

2 Data

In this study, we employ solar wind and geomagnetic measurements obtained from the

NASA OMNI database, which provides a comprehensive, cross-calibrated, and time-shifted collection of interplanetary plasma and magnetic field parameters. The OMNI dataset compiles measurements from several spacecraft located either in geocentric orbit or near the Sun–Earth L1 Lagrange point, including IMP-8, Wind, Geotail, and the Advanced Composition Explorer (ACE) [17,32]. The OMNI processing applies cross-comparison, cross-normalization, and standard time-shifting of solar wind measurements to the Earth's bow shock nose to ensure consistency and accurate timing relative to magnetospheric responses. These procedures make OMNI one of the most reliable sources for long term space weather analysis. All data used in this study were obtained from the OMNIWeb interface (`https://omniweb.gsfc.nasa.gov/`). We utilize eight key solar wind parameters from OMNI dataset:the magnitude of the interplanetary magnetic field, $|B|$ (nT); the GSM components of the IMF, B_x, B_y, and B_z (nT); the radial solar wind velocity, V_x (km s^{-1}); the proton temperature, T (K); the proton number density, N_p (cm^{-3}); the bulk solar wind flow speed, V_{flow} (km s^{-1}); and the global geomagnetic index K_p. These parameters are provided as hourly averages, processed from higher resolution measurements using standard arithmetic averaging, consistent with the approach commonly adopted in long term solar–terrestrial studies. The K_p index is derived from three hourly measurements recorded at 13 mid latitude geomagnetic observatories [33]. It characterizes fluctuations in the horizontal component of Earth's magnetic field on a quasi-logarithmic scale from 0 (quiet) to 9 (extreme storm), with values ≥ 5 indicating geomagnetic storm conditions. We use the hourly averaged K_p values provided by OMNIWeb. The dataset spans January 1999 to December 2024, covering the descending phase of Solar Cycle 23, the complete duration of Solar Cycle 24, and the rising phase of Solar Cycle 25. This extended interval includes periods of both high and low solar activity, enabling a robust investigation of solar wind–geomagnetic coupling across multiple solar cycles.

Figure 1 presents the temporal evolution of the solar wind and geomagnetic parameters used in this study during the selected interval in May 2024 (from 7–15 May 2024, the Sun exhibited elevated activity, including multiple X- and M-class solar flares and launched several coronal mass ejections (CMEs) toward Earth).

3 Methodology

3.1 Sliding Time Window Construction

In statistical time series forecasting, the concept of historical memory is mathematically implemented through a sliding window technique [27,34]. To transform the continuous solar wind time series into supervised learning samples, we apply a sliding window approach. At each time step, the model uses a fixed length (w) history of solar wind parameters to predict the future value of the K_{p} index. We denote the solar wind data (X) with size $\tau \times F$, where in our data, the number of time step is $\tau = 227928$ and the number of solar wind features is $F = 8$. Each input sample consists of w consecutive hours of solar wind data, and the corresponding target is the K_{p} value at the next hour. The window is shifted forward by one time step to generate overlapping samples, ensuring that all available temporal information is utilized. Figure 2 represents a schematic representation of the multivariate sliding window mechanism for $w = 6$. Each three blocks (w_1, w_2, w_3) illustrates a distinct 6 hour temporal sequence matrix comprising 8 parallel solar wind features (S_1 to S_8). At each iteration, the window slides forward by a one hour step, updating the historical input sequence (e.g., from $t_1 \ldots t_6$ to $t_2 \ldots t_7$) to forecast the immediate subsequent geomagnetic target, yielding $K_{\text{p}}(7)$, $K_{\text{p}}(8)$, and $K_{\text{p}}(9)$, respectively. In this regard, for example of a w size window, we

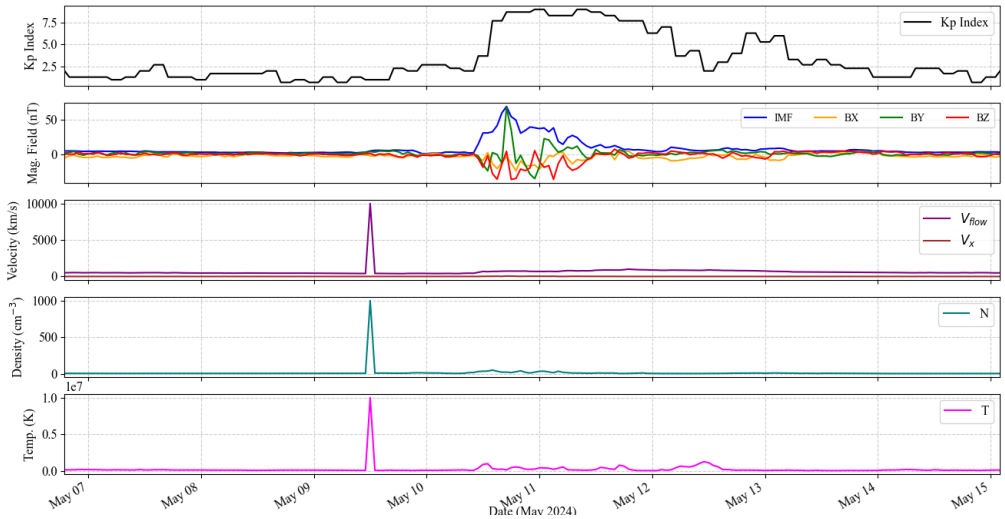

Figure 1: Time series of the parameters used in this study during May 2024, including the geomagnetic index K_p, the magnitude of the interplanetary magnetic field $|B|$ and its GSM components (B_x, B_y, B_z), the solar wind velocities (V_{flow} and V_x), the proton number density N_p, and the proton temperature T.

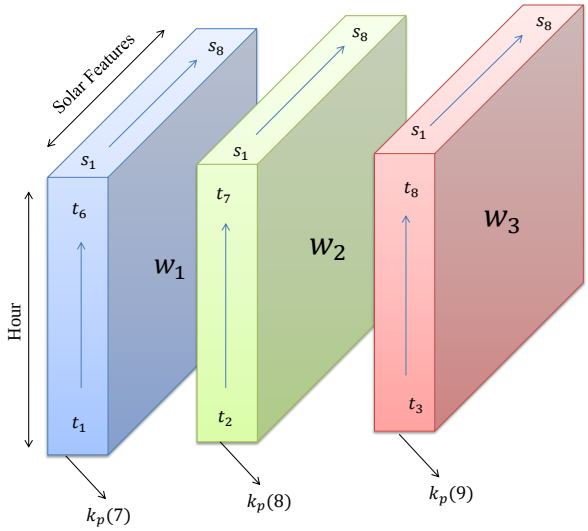

Figure 2: Schematic illustration of the multivariate sliding window framework with window length $w = 6$. Each block (w_1, w_2, w_3) represents a 6 hour temporal sequence matrix composed of eight concurrent solar wind features (S_1–S_8). The window advances by one hour at each step, updating the input sequence from $t_1 \dots t_6$ to $t_2 \dots t_7$ and $t_3 \dots t_8$, while predicting the subsequent geomagnetic index values $K_{\text{p}}(7)$, $K_{\text{p}}(8)$, and $K_{\text{p}}(9)$, respectively.

have a 3D array consisting of $N = \tau - w$ windows, each window containing 8 solar wind features and has a target K_{p}. We perform the procedure for $w = 6, 12, 24, 72, 120$.

3.2 Long Short Term Memory (LSTM) neural network Architecture

We apply a supervised deep learning approach based on a stacked LSTM recurrent neural network to model the relationship between multivariate solar wind inputs and the target K_p index. The machine incorporates temporal dependencies by transforming the data into sliding windows of fixed length, where each sample consists of a sequence of past observations used to predict the subsequent target value. The model architecture comprises two sequential LSTM layers with recurrent dropout regularization to capture short and long term temporal dynamics [35], followed by fully connected layers with rectified linear unit (ReLU) activations for nonlinear feature transformation [36]. A final linear output layer produces continuous predictions, enabling a regression formulation. Model parameters are optimized using the Adam optimizer with mean squared error as the loss function [37]. Early stopping and adaptive learning rate reduction are employed to improve generalization and stabilize convergence.

3.3 Network Architecture and Training Configuration

To promote reproducibility and methodological consistency, we apply a unified experimental protocol to all examined temporal window configurations. The 25 year continuous dataset is divided chronologically to maintain the natural temporal order of the observations. The initial 80% of the data is allocated for model development, while the remaining 20% served as an independent test set for evaluating predictive generalization. To eliminate the risk of data leakage, we derive normalization parameters (mean and standard deviation) solely from the training subset and subsequently apply to the entire dataset. The predictive framework is based on a deep stacked LSTM architecture composed of two consecutive LSTM layers with 128 and 64 hidden units, respectively. Regularization is introduced through recurrent dropout (0.1) within the LSTM layers and standard dropout (0.15) between layers to reduce overfitting. The recurrent component is followed by two fully connected dense layers containing 128 and 64 neurons with ReLU activation functions, and a final linear layer that outputs continuous predictions. Training them to using mini batches of 128 sequences over a maximum of 60 epochs. To enhance training stability and prevent overfitting, early stopping with a patience of 6 epochs is employed. In addition, an adaptive learning rate scheduling mechanism is implemented, reducing the learning rate when performance stagnates for 3 consecutive epochs.

The complete architecture and forward propagation mechanism of the proposed LSTM network are illustrated in Figure 3. The model processes the multidimensional solar wind features through a continuous 6 hour historical input window. The sequential learning is driven by two stacked LSTM layers, configured with 128 and 64 units, respectively. To mitigate overfitting, a dropout rate of 0.15 is applied after each recurrent layer. The extracted temporal features are then mapped to the target variable through two fully connected dense layers (128 and 64 units) equipped with ReLU activation functions. Finally, a single node output layer with linear activation generates the scaled prediction, which subsequently undergoes an inverse scaling transformation to recover the actual K_p index values.

3.4 Evaluation Metrics

Model performance across different input window lengths was quantitatively evaluated using four widely adopted statistical indicators. Forecasting geomagnetic indices involves inherently complex and non gaussian data characteristics; therefore, combining metrics based on

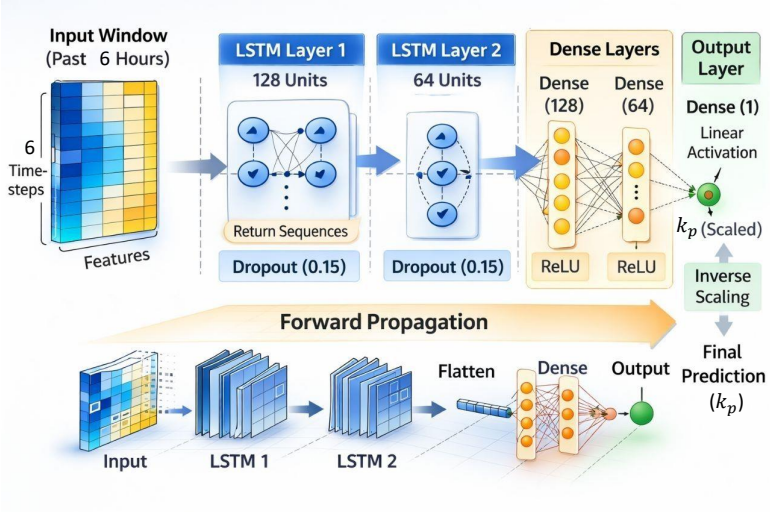

Figure 3: Detailed schematic of the proposed LSTM architecture for K_{p} index forecasting. The upper panel details the specific layer configurations, hidden units, and dropout regularization, while the lower panel visually represents the forward propagation of features from the 6 hour input window to the final inversely scaled prediction.

both squared and absolute deviations provides a more complete assessment of predictive accuracy [38]. The evaluation framework includes Mean Squared Error (MSE), Root Mean Square Error (RMSE), Mean Absolute Error (MAE), and the Coefficient of Determination (R^2), defined as:

$$MSE = \frac{1}{N}\sum_{i=1}^{N}(y_i - \hat{y}_i)^2 \tag{1}$$

$$RMSE = \sqrt{\frac{1}{N}\sum_{i=1}^{N}(y_i - \hat{y}_i)^2} \tag{2}$$

$$MAE = \frac{1}{N}\sum_{i=1}^{N}|y_i - \hat{y}_i| \tag{3}$$

$$R^2 = 1 - \frac{\sum_{i=1}^{N}(y_i - \hat{y}_i)^2}{\sum_{i=1}^{N}(y_i - \bar{y})^2} \tag{4}$$

Here, N denotes the number of sequential samples in the test dataset, y_i represents the observed geomagnetic index, $\hat{y}_i$ is the corresponding model prediction, and $\bar{y}$ indicates the mean value of the observed data.

4 Results and Discussion

We apply an LSTM based machine learning model to predict variations in the K_p geomagnetic index using eight solar wind parameters as inputs. We use a sliding window approach to the temporal time series data to capture sequential dependencies between upstream solar wind conditions and geomagnetic responses. The model is trained and evaluated by comparing predicted values with observed measurements, with emphasis on its ability to reproduce short term fluctuations and overall trend behavior.

4.1 Performance Across Temporal Windows

During the experimental stage, we evaluate the predictive performance of the LSTM model using multiple historical input window lengths (w). We test sliding temporal windows of 6, 12, 24, 48, 72, and 120 hours to assess how the extent of prior solar wind information influences forecasting skill. Table 1 presents the statistical performance metrics—MSE, RMSE, MAE, and R^2—for each configuration. The results demonstrate that the 6 hour input window ($w = 6$) provides the most accurate predictions among all tested configurations. This setting yields the highest coefficient of determination ($R^2 = 0.7233$) together with the lowest error values (MSE = 0.4350, RMSE = 0.6596, MAE = 0.4947). As shown in Table 1, increasing the input window beyond 24 hours generally leads to a reduction in predictive performance, reflected by lower R^2 values and higher error magnitudes. From a modeling standpoint, the LSTM architecture captures temporal dependencies by learning from sequential historical inputs. Although LSTMs are designed to retain long term contextual information, the evaluation indicates that incorporating solar wind data extending beyond approximately one day introduces information that does not improve—and may hinder—predictive capability. Longer sequences appear to introduce redundant or weakly relevant patterns, which can obscure the model's ability to learn the most influential nonlinear relationships between solar wind drivers and geomagnetic responses. The identification of a 6 hour optimal window is consistent with earlier localized investigations, including the architecture proposed by Tan et al. (2018) [23], which also emphasized short term dependencies. By extending the analysis across a continuous 25 year dataset (1999–2024) encompassing multiple solar cycles, the present study shows that this short memory scale represents a robust dynamical feature of the magnetosphere rather than a dataset specific outcome. Furthermore, while the obtained error metrics (RMSE = 0.6596, MAE = 0.4947) are competitive with historical neural network benchmarks [22,23], the systematic window length evaluation establishes a clearer physical and statistical boundary: providing historical input beyond 24 hours not only yields diminishing returns but also actively weakens predictive performance by introducing outdated interplanetary conditions.

From a physical standpoint, the 6 hour optimal window aligns closely with characteristic timescales of solar wind–magnetosphere energy transfer. The solar wind requires approximately one hour to propagate from the L1 Lagrange point to Earth, depending on its bulk radial velocity [3]. Following arrival, geomagnetic responses—such as magnetic field reconfiguration and fluctuations represented by the K_p index—develop over several hours [39]. Therefore, a 6 hour continuous window effectively captures the immediate upstream conditions, propagation delay, and transient magnetospheric response, indicating that geomagnetic variability is primarily governed by recent solar wind drivers rather than extended historical conditions.

Table 1: Performance evaluation of the LSTM model across different input window lengths (w). The 6 hour window yields the most accurate statistical predictions.

Window (w)	MSE	RMSE	MAE	R^2
6h	0.4350	0.6596	0.4947	0.7233
12h	0.4655	0.6823	0.5067	0.7039
24h	0.4519	0.6723	0.5025	0.7125
48h	0.4776	0.6911	0.5183	0.6962
72h	0.4581	0.6768	0.5078	0.7086
120h	0.4661	0.6827	0.5099	0.7036

4.2 Overall Prediction Accuracy

To evaluate the global predictive performance of the optimized 6 hour model across the full test dataset (comprising more than 45,000 continuous temporal sequences), we perform a hexagonal binning density analysis. Figure 4 illustrates the relationship between predicted and observed values, where the color scale represents the frequency of data points within each bin. The highest density regions (darker shading) are concentrated near the ideal prediction line ($y = x$), indicating strong agreement between model predictions and observations for low to moderate geomagnetic activity levels ($K_\mathrm{p} < 5$). The density structure also reveals the heavy tailed nature of the dataset, where extreme geomagnetic conditions ($K_\mathrm{p} \geq 7$) occur infrequently and appear in sparsely populated regions of the distribution. Within these low density regions, the model shows a slight tendency to underestimate peak values, which is a common statistical behavior when modeling highly imbalanced natural datasets.

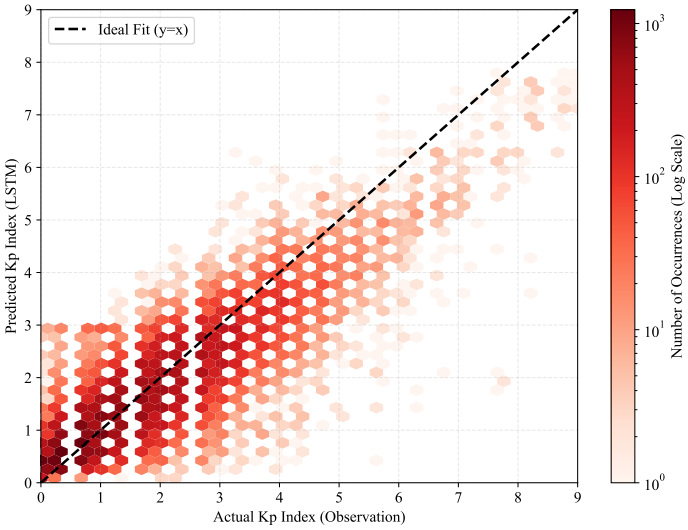

Figure 4: Hexagonal binning density plot illustrating the correlation between actual K_p observations and LSTM predictions for the optimal 6 hour window. The color gradient indicates the frequency of occurrences, highlighting the model's accuracy in high density regions and the rarity of extreme events. The dashed line represents the ideal fit.

As illustrated by the density distribution in Figure 4, the overall correlation remains

strong ($R^2 = 0.7233$), while extreme peaks are slightly underestimated. Extreme geomagnetic fluctuations follow a heavy tailed distribution and occur far less frequently than quiet or moderate conditions in the 25 year dataset. Consequently, regression based learning algorithms optimize model parameters to minimize global error metrics (e.g., MSE), which statistically biases predictions of rare extreme events toward the mean state.

Figure 5 shows a time series comparison between the observed K_p index (solid blue line) and the values predicted by the LSTM model (dashed orange line) over a selected interval. The model reproduces the overall temporal evolution of geomagnetic activity, capturing both gradual variations and rapid disturbances with good phase agreement. The timing of the major storm event is well represented, and the predicted curve follows the rise and decay pattern of the observation. However, a noticeable deviation occurs during the most intense interval, where the observed peak reaches the maximum level ($K_p = 9$), while the model underestimates the magnitude of this extreme event. This discrepancy reflects a limitation in peak amplitude reconstruction under severe geomagnetic conditions, despite the model maintaining consistent performance during moderate and quiet periods.

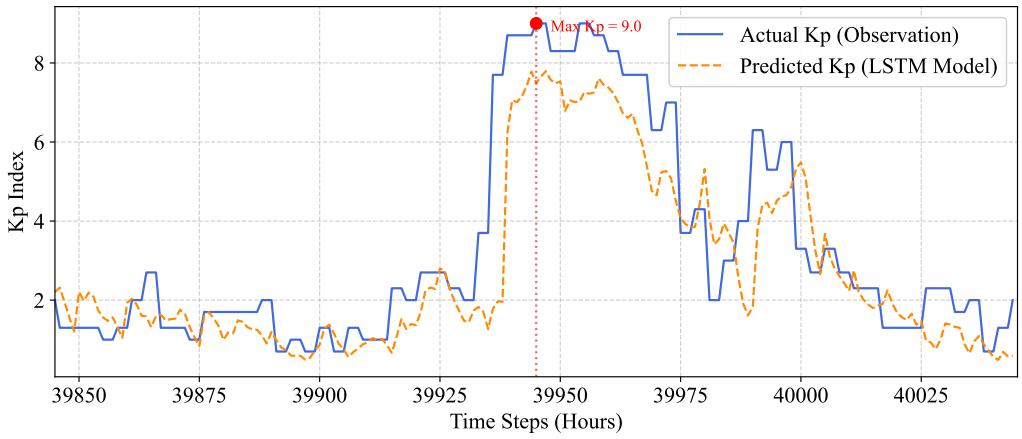

Figure 5: Time series visualization of the LSTM model's performance during a period of severe geomagnetic variation. The network captures the non linear dynamical jump based on the 6 hour solar wind history.

5 Conclusion

Our LSTM based model proves effective at predicting short term variations in the K_p geomagnetic index using upstream solar wind data. By systematically testing different input window lengths, we found that a 6 hour historical window works best, striking the right balance between predictive accuracy and capturing the most relevant recent solar wind conditions. Longer histories tend to add redundant or less useful information, which can actually reduce the model's performance.

With this 6 hour setup, the model shows strong agreement with observations across a 25 year dataset ($R^2 = 0.7233$), successfully capturing both gradual trends and moderate geomagnetic fluctuations. While extreme events are slightly underestimated—understandable given their rarity—the model reliably reproduces the timing and overall structure of ma-

jor disturbances. Overall, these results suggest that when LSTMs are tuned to focus on short term dependencies, they offer a physically meaningful and statistically robust tool for forecasting geomagnetic activity, effectively linking upstream solar wind conditions to the dynamic response of Earth's magnetosphere.

Acknowledgment

The authors would like to express their gratitude to the developers of the NASA OMNIWeb database for providing the high resolution space physics data essential for this research. The authors acknowledge the use of artificial intelligence tools for language editing of the manuscript.

Authors' Contributions

All authors have contributed equally to the conceptualization, methodology, software development, and writing of this manuscript. The historical solar wind and K_{p} index data that support the findings of this study are openly available in the NASA OMNIWeb database at `https://omniweb.gsfc.nasa.gov/`.

Conflicts of Interest

The authors declare that there is no conflict of interest regarding the publication of this paper.

Ethical Considerations

The authors have diligently addressed ethical concerns, such as informed consent, plagiarism, data fabrication, misconduct, falsification, double publication, redundancy, submission, and other related matters.

Funding

This research did not receive any specific grant from funding agencies in the public, commercial, or not for profit sectors.

References

[1] Rangarajan, G. K., & Barreto, L. M. 1999, Earth, Planets and Space, 51, 363.

[2] Matzka, J., et al. 2021, Space Weather, 19, e2020SW002641.

[3] Elliott, H. A., et al. 2013, Space Weather, 11, 339.

[4] Lockwood, M., et al. 2017, Journal of Space Weather and Space Climate, 7, A25.

[5] Chakraborty, S., & Morley, S. K. 2020, Journal of Space Weather and Space Climate, 10, 36.

[6] Zhang, J., et al. 2007, Journal of Geophysical Research (Space Physics), 112, A10102.

[7] Saiz, E., et al. 2013, Journal of Space Weather and Space Climate, 3, A26.

[8] Kim, S., Li, X., Damas, M. C., & Ngwira, C. 2017, AGU Fall Meeting Abstracts, Vol. 2017 of AGU Fall Meeting Abstracts, ED11D.

[9] Osmane, A., et al. 2015, Journal of Geophysical Research (Space Physics), 120, 9307.

[10] Boroyev, R. N. 2019, Advances in Space Research, 63, 302.

[11] Lazzeri, C., et al. 2024, European Geosciences Union General Assembly 2024 (EGU24), EGU General Assembly Conference Abstracts

[12] Lockwood, M. 2022, Space Weather, 20, e2021SW002989.

[13] Tasnim, S., et al. 2025, Frontiers in Astronomy and Space Sciences, 12, 1675769.

[14] Liu, W., et al. 2021, 101st Annual AMS Meeting 2021, Vol. 101 of American Meteorological Society Meeting Abstracts PUBLISHER , p. Joint.

[15] Masuda, A., Hebishima, H., & ichi Inage, S. 2026, Next Sustainability, 7, 100225.

[16] Camporeale, E. 2019, Space Weather, 17, 1166.

[17] Detman, T., & Joselyn, J. 1999, Solar Wind Nine, Vol. 471 of American Institute of Physics Conference Series, edited by Habbal, S. R., Esser, R., Hollweg, J. V., & Isenberg, P. A. AIP , 729.

[18] Lockwood, M., et al. 2020, Journal of Space Weather and Space Climate, 10, 23.

[19] Khabarova, O., & Price, C. 2024, Frontiers in Astronomy and Space Sciences, 11, 1493917.

[20] Lazzeri, C., et al. 2024, Journal of Geophysical Research (Space Physics), 129, e2023JA032160.

[21] Boberg, F., Wintoft, P., & Lundstedt, H. 2000, Physics and Chemistry of the Earth, Part C: Solar, Terrestrial & Planetary Science, 25, 275.

[22] Wing, S., et al. 2005, Journal of Geophysical Research: Space Physics, 110.

[23] Tan, Y., Hu, Q., Wang, Z., & Zhong, Q. 2018, Space Weather, 16, 406.

[24] Zhelavskaya, I. S., Shprits, Y. Y., & Spasojević, M. 2019, Space Weather, 17, 1016.

[25] Gruet, M. A., Chandorkar, M., Sicard, A., & Camporeale, E. 2018, Space Weather, 16, 1882.

[26] Conde, D., et al. 2023, Space Weather, 21, e2023SW003474, e2023SW003474 2023SW003474.

[27] Azlan, A., Yusof, Y., & Mohsin, M. F. M. 2019, International Journal of Advanced Computer Research, 9, 260.

[28] Houndekindo, F., & Ouarda, T. B. M. J. 2025, Energy, 328, 136498.

[29] Alguhi, A. A., & Al-Shaalan, A. M. 2025, Energies, 18, 4594.

[30] Jeon, E., Jin, D., & Kim, Y. 2026, Machines, 14, 135.

[31] Javaherian, M., et al. 2025, Scientific Reports, 15, 44006.

[32] Stone, E. C., et al. 1998, Space Sci. Rev., 86, 1.

[33] Wang, J., et al. 2015, Space Weather, 13, 831.

[34] Hassani, Z., Mohammadpur, D., & Safari, H. 2025, ApJS, 279, 27.

[35] Hochreiter, S., & Schmidhuber, J. 1997, Neural computation, 9, 1735.

[36] Goodfellow, I. Deep learning, 2016.

[37] Kingma, D. P., & Ba, J. 2014, arXiv preprint arXiv:1412.6980,

[38] Chakraborty, S., & Morley, S. K. 2020, Journal of Space Weather and Space Climate.

[39] Lin, J.-W. 2021, European Journal of Geosciences.